Malaysian Applied Biology (2024) 53(6): 143-155
https://doi.org/10.55230/mabjournal.v53i6.1

Research

Antimicrobial Activity, *In Silico* Analysis, and Molecular Docking Studies of An Iodide-Bridged Dimeric Palladium Complex: A Comprehensive Insight

Nur Anis Nabilah Mohd Fuzi[1], Khairil Anuar Jantan[1]*, Amirul Ridzuan Abu Bakar[2], Nik Muhammad Azhar Nik Daud[2], Mohammad Noor Jalil[1], Hamizah Mohd Zaki[1], Jamil Mohamed Sapari[3], Shamsul Bahrin Gulam Ali[4]*

1. School of Chemistry and Environment, Faculty of Applied Sciences, Universiti Teknologi MARA, 40450 Shah Alam, Selangor, Malaysia
2. Faculty of Chemical Engineering and Technology, Universiti Malaysia Perlis, Kompleks Pusat Pengajian, Jejawi 3, Arau, Perlis, Malaysia
3. School of Chemistry and Environment, Faculty of Applied Sciences, Universiti Teknologi MARA, Negeri Sembilan Branch, Kuala Pilah Campus, 72000 Kuala Pilah, Negeri Sembilan, Malaysia
4. Faculty of Health Sciences, Bertam Campus, Universiti Teknologi MARA, 13200 Kepala Batas, Penang Malaysia

*Corresponding author: khairil0323@uitm.edu.my; sbahrin@uitm.edu.my

ABSTRACT

The iodide-bridged dimeric palladium complex $[N^nBu_4]_2[Pd_2I_6]$ was synthesized and characterized using various physiochemical analyses, including elemental and thermal analysis, UV-Vis, FTIR, and NMR spectroscopy. The antibacterial activity of the compound was evaluated using the disk diffusion method against a panel of bacteria, demonstrating broad-spectrum effectiveness against two Gram-positive bacteria (*Bacillus cereus* & *Bacillus subtilis*) and four Gram-negative bacteria (*Salmonella typhimurium, Escherichia coli, Klebsiella aerogenes* & *Klebsiella pneumoniae*). Molecular docking studies revealed a calculated binding energy score of -9.90 kcal/mol against the Thymidylate Kinase (TMK) protein, suggesting potential interaction and affinity. Physicochemical parameters, as the Swiss ADME web server predicted, indicated limited permeability across the blood-brain barrier and no gastrointestinal absorption. The Lipinski and Egan models predicted favorable drug-like characteristics for $[N^nBu_4]_2[Pd_2I_6]$. $[N^nBu_4]_2[Pd_2I_6]$ was classified as Toxicity Class 3 for acute oral toxicity, with an LD_{50} value of 189 mg/kg. Predictive modeling using the ProTox-III web server yielded an average similarity of 88% and prediction accuracy of 71%. In conclusion, the obtained biological data suggest that $[N^nBu_4]_2[Pd_2I_6]$ could be a promising candidate for future development as an antibacterial agent.

Key words: Antibacterial activity, *in silico* study, molecular docking, palladium complex

Article History
Accepted: 4 September 2024
First version online: 25 December 2024

Cite This Article:
Mohd Fuzi, N.A.N., Jantan, K.A., Abu Bakar, A.R., Nik Daud, N.M.A., Jalil, M.N., Mohd Zaki, H., Mohamed Sapari, J. & Gulam Ali, S.B. 2024. Antimicrobial activity, in silico analysis, and molecular docking studies of an iodide-bridged dimeric palladium complex: A comprehensive insight. Malaysian Applied Biology, 53(6): 143-155. https://doi.org/10.55230/mabjournal.v53i6.1

INTRODUCTION

The pressing requirement to develop potent antimicrobial agents is an essential priority in the healthcare industry, owing to the significant threat to public health posed by the rise of antibiotic-resistant microorganisms (Dhingra *et al*., 2020). One promising approach to address this challenge is the exploration of metal-based complexes, such as palladium (Pd) complexes, as potential antimicrobial agents (Frei *et al*., 2020). The growing fascination with metal-based treatments, particularly Pd complexes, has been fueled by a more profound comprehension of the reactivity of metal ions and their interactions with biomolecules, such as DNA and proteins (Soldevila-Barreda & Metzler-Nolte, 2019). Pd complexes have been documented to possess potent antimicrobial properties (Zalevskaya *et al*., 2020; Aljohani *et al*., 2021) due to their capacity to disrupt the biological processes of microbes. This disruption includes interfering with DNA replication, decreasing enzyme activity, and producing oxidative stress (Frei *et al*., 2023). Pd complexes have demonstrated a preference for targeting microbial cells

while causing minimum harm to human cells, which makes them a promising choice for therapeutic advancement (Oliveira *et al*., 2014). Innovative therapeutic medications' logical development and enhancement are facilitated by comprehending the binding interactions between Pd complexes and their target proteins through *in silico* and molecular docking techniques (Dechouk *et al*., 2022).

Molecular docking holds great promise for identifying new therapeutic targets and developing safe and effective treatments for various diseases (Agu *et al*., 2023). Hence, in this study, molecular docking was performed to fathom the chemical interaction between $[N^nBu_4]_2[Pd_2I_6]$ complex and the protein of *Staphylococcus aureus,* thymidylate kinase (TMK). The TMK was selected for docking studies due to its critical role in bacterial DNA synthesis and cell division. TMK catalyzes the phosphorylation of thymidine monophosphate (dTMP) to thymidine diphosphate (dTDP), an essential step in the nucleotide biosynthesis pathway. Inhibiting TMK disrupts the production of dTTP, leading to impaired DNA replication and cell proliferation, which is particularly detrimental to bacteria, making TMK a promising target for antibacterial agents (Jayanthi & Azam, 2023). Targeting bacterial TMK can minimize potential off-target effects on human cells, as TMK is a conserved enzyme in many bacteria but has enough structural differences from the human enzyme to allow for the development of selective inhibitors. This selective inhibition is crucial for developing antibacterial agents that are effective against bacterial infections and safe for human use. Researchers can design inhibitors targeting the bacterial enzyme by focusing on the structural differences between bacterial and human TMK while minimizing off-target effects. This approach underscores the importance of TMK as a strategic target in developing new antibacterial therapies (Kawatkar *et al*. 2014). An ADMET study was also completed to forecast toxicity and pharmacokinetic profiles of the $[N^nBu_4]_2[Pd_2I_6]$ complex.

However, the availability and cost of Pd are limiting factors that impede its use as a medical antibacterial agent, especially when significant quantities are required (Balaram, 2019). Approximately 80% of global Pd consumption is attributed to the automotive sector, particularly in producing three-way catalysts (TWCs) (Cowley, 2022). Unfortunately, the catalytic activity of TWC declines and becomes inactive within 8-10 years (Gombac *et al*., 2016) due to various reasons, including fouling, poisoning, heat degradation, and sintering (Moulijn *et al*., 2001). The disposal of spent TWCs was anticipated to have a significant environmental impact due to the direct disposal of a substantial quantity of valuable metal into landfills (Robinson, 2009). Serpe *et al*. (2005) published a study focusing on Pd recovery methods that are less harmful to the environment. The dithiooxamide lixiviant, Me_2dazdt.$2I_2$ (Me_2dazdt = N, N′-dimethyl-perhydrodiazepine-2,3-dithione) successfully recovered 90% of Pd from model TWCs. However, this method requires Lawesson's reagent to generate Me_2dazdt ligand and demands a longer reaction time to achieve Pd dissolution; nevertheless, it remains practical (Jantan *et al*., 2017). A cost-effective and readily accessible technique has been devised to selectively extract Pd from used TWC (Figure 1), ensuring safety and sustainability by using iodine with tetrabutylammonium iodide; $[N^nBu_4]I$ forming iodide-bridged dimeric palladium complex through precipitation (Cuscusa *et al*., 2017). Nevertheless, converting the Pd content of $[N^nBu_4]_2[Pd_2I_6]$ into its metallic form remains energy-intensive and expensive. As a result, current research efforts are directed towards valorizing the compound directly to promote a 'circular economy.' Indeed, recent findings suggest that the iodide-bridged dimeric palladium complex can catalyze C-H oxidative functionalization and C-N amination (Jantan *et al*., 2024).

Given the well-established recovery procedure and the plethora of information on treating spent TWC material with $[N^nBu_4]I$ and I_2 to produce $[N^nBu_4]_2[Pd_2I_6]$ with high efficiency (Figure 1), the current project will not focus on this aspect. Instead, palladium powder will be utilized as a substitute for TWC material. This study intends to directly valorize $[N^nBu_4]_2[Pd_2I_6]$ as an effective antibacterial agent against various human pathogenic microorganisms.

MATERIALS AND METHODS

Reagents

All the chemicals and solvents (analytical-grade quality) were obtained and used without additional purification unless specifically stated. Tetrabutylammonium iodide, iodine, and Pd powder were obtained from Sigma-Aldrich. Acetone, dichloromethane, diethyl ether, and ethanol were supplied by Merck.

Physical measurements

Elemental analysis was performed using a Model 2400 Perkin-Elmer Series II CHNS/O analyzer, accurately detecting the presence of carbon, hydrogen, and nitrogen in the sample. Melting points were determined in open glass capillaries on Stuart SMP10 melting point apparatus equipped with a microscope. The FT-IR spectra corresponding to significant functional groups were obtained using a Nicolet 6700 spectrometer (Thermo Fisher Scientific) equipped with a versatile Attenuated Total

Reflectance (ATR) sampling accessory with a diamond crystal plate. The infra-red spectra were recorded in the 4000 to 600 cm^{-1} spectral range with 16 sample/background scans using OMNIC 8.1 computer software.

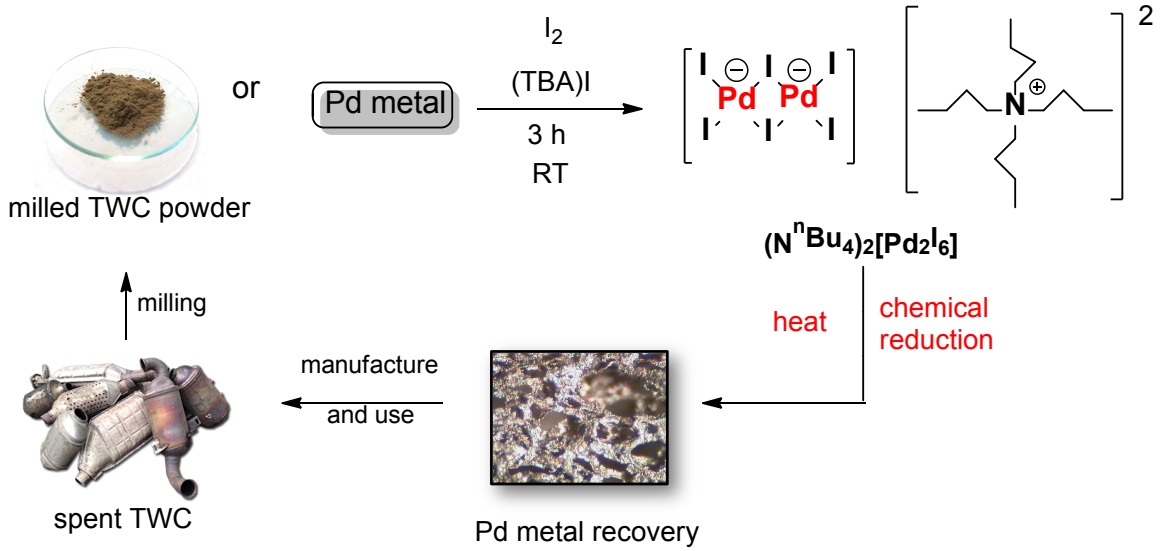

Fig. 1. Palladium leaching from spent three-way catalytic converters

NMR spectra were acquired at ambient temperature using a 400 MHz JEOL spectrometer (JNM-ECZS) (400 MHz for ^{1}H NMR, & 100 MHz for $^{13}C\{^{1}H\}$ NMR). Electronic spectral changes reflecting electron distribution between ligand-metal in the compound were recorded at 25°C on Lambda-25 UV-Vis Spectrophotometer (Perkin Elmer) using a UV quartz cell of 10 mm path length. The spectra were acquired with multiple scans between 300–800 nm wavelength. The mass-loss data were examined using a Mettler Toledo TGA/DSC 1LF/UMX Thermogravimetric Analyzer, heated from 30°C to 550°C at a rate of 10°C per min under a nitrogen environment.

Synthesis of the palladium complex

Tetrabutylammonium iodide, $[N^{n}Bu_4]I$ (71.20 mg, 0.2 mmoL), and I_2 (50.86 mg, 0.2 mmoL) were dissolved in an acetone solution (30 mL). The Pd metal powder (20.74 mg, 0.2 mmoL) was then added to the reaction mixture and stirred for 3 hr at room temperature. The initially brown solution gradually darkened during the reaction, resulting in the formation of abundant black crystalline precipitates. The product was isolated by filtration, washed with diethyl ether (10 mL), and air-dried. Additional precipitate was obtained by layering the filtrate with diethyl ether. A minor adjustment was made to expedite the synthesis process by introducing 20 mL of ethanol into the reaction mixture after 3 hr. The solvent was concentrated using a rotary evaporator, yielding a solid product in the remaining ethanol solution. The product was then filtered and washed with diethyl ether (Jantan *et al.*, 2024). The spectroscopic data obtained from the product are consistent with the established analytical procedure.

Antibacterial studies – disk diffusion method

The antibacterial potential of $[N^{n}Bu_4]_2[Pd_2I_6]$ was evaluated using the disk diffusion method against six bacterial strains: two Gram-positive (*Bacillus cereus* ATCC11778 and *Bacillus subtilis* ATCC13124) and four Gram-negative (*Escherichia coli* ATCC25922, *Salmonella typhimurium* ATCC14028, *Klebsiella pneumoniae* ATCC700603 and *Klebsiella aerogenes* ATCC13048). Bacterial strains were cultured at 37°C on a nutrient agar medium (Oxoid, UK). Gram staining and observation of colony morphology were performed to confirm the identity of the working strains. An overnight culture of each microbe was incubated at 37°C in Mueller-Hinton agar (MHA) and used as the inoculum. The bacterial culture was adjusted to 0.5 McFarland standard in visible turbidity to achieve a 1.5×10^{8} CFU/mL concentration in normal nutrient broth.

Sterile cotton swabs were used to evenly streak MHA plates, which were then air-dried under laminar flow in a fume hood. Sterile paper disks (6 mm) were prepared using Whatman No. 1 filter paper to mimic the conventional antibiotic disks and were placed on the surface of the MHA plates, with each plate containing four disks spaced equidistantly. The tested compound was solubilized in

dichloromethane (DCM) to obtain desired concentrations (1, 2, 3 & 4 mg/mL) and filtered through 0.45 µm Millipore filters for sterilization. Each disk was impregnated with 20 µL of the respective compound concentration.

A standard commercial antibiotic disk (Gentamicin 10 µg) served as the positive control, while a disk impregnated with sterile distilled water served as the negative control. The plates were then incubated overnight at 37°C. Following incubation, the antibacterial activity was assessed by measuring the zone of inhibition against the tested organisms. All assays were performed in triplicate per condition according to our previously reported method (Fuzi *et al*., 2023).

Determination of Minimum Inhibitory Concentration (MIC) and Minimum Bactericidal Concentration (MBC)

The broth macro dilution method was employed to ascertain the MIC of the complex against the bacterial cultures being studied. The inoculum was prepared and adjusted visually to 0.5 McFarland standard following the indicated procedure. Eight sterile test tubes were each inoculated with 1 mL of adjusted inoculum. 1 mL of CH_2Cl_2 solution containing complex was added into the first tube, and two-fold serial dilutions were performed, resulting in a final concentration range from 10 mg/mL to 0.078 mg/mL. Two additional tubes were prepared as positive growth control (MHB + bacteria) and negative control (MHB only). Each experiment was performed in triplicate and was incubated overnight at 37°C. The MIC was determined to be the lowest complex concentration that inhibited visible growth. The turbidity of the tubes was visualized before and after incubation to determine the MIC value, where turbidity post-incubation indicates visible growth of microorganisms. For MBC, the MIC tubes that showed no apparent visible growth were subcultured onto the MHA plate for a further 24 hr of incubation. Following incubation, no evidence of bacterial growth was confirmed as MBC values (Fuzi *et al*., 2023).

Statistical analysis

The collected data were subjected to statistical analysis using GraphPad Prism 8.0 software. The results are presented as means ± standard error of the mean (SEM) for the inhibitory zone. Each value represents the mean of three independently conducted experiments, accompanied by its respective SEM. Subsequent analysis involved a two-way Analysis of Variance (ANOVA) followed by Tukey's multiple comparison post-test. All statistical tests determined significance at a threshold of $p<0.05$, with asterisks used to denote statistically significant differences.

ADMET analysis

The compound $[N^nBu_4]_2[Pd_2I_6]$ underwent computational assessment of its ADME (absorption, distribution, metabolism & excretion) profiles and drug-likeness parameters using the publicly accessible online tools SwissADME (Daina *et al*., 2017) and admetSAR (Yang *et al*., 2019). Various physicochemical properties were analyzed, including lipophilicity, water solubility, and pharmacokinetics. Drug-likeness was evaluated based on established criteria such as Lipinski's (Lipinski *et al*., 1997), Veber's (Veber *et al*., 2002), Ghose's (Ghose *et al*., 1999), Egan's (Egan *et al*., 2000), and Muegge's (Muegge, 2002) rules. Additionally, toxicity prediction was performed using the ProTox-3 application to estimate LD_{50} endpoints and toxicity classes (Drwal *et al*., 2014).

Molecular docking

The monomeric structure of Thymidylate Kinase (TMK) from *Staphylococcus aureus* (PDB ID: 4GFD, resolution: 1.80 Å) was obtained from the Protein Data Bank (www.rcsb.org) and utilized for molecular docking analysis. The structure of $[N^nBu_4]_2[Pd_2I_6]$ was constructed as an sdf.file using ChemDraw, and Open Babel software was employed to convert the structure into PDB format. Molecular docking studies were conducted using AutoDock 4.2 software (Morris *et al*., 2009) with modifications to the AD4_ parameters.dat file to incorporate atomic parameters for palladium. Configuration files for the protein were prepared with specific Cartesian coordinates to define the docking grid. Initially, blind docking was conducted to identify the favorable binding site inside the protein region. Upon identification of the binding site, localization of the docking binding site was conducted. In this setting, the binding site grid was defined with dimensions of 50 x 50 x 50 points, centered at coordinates (8.277, -7.845, 1.834) Å, and a grid spacing of 0.375 Å. Docking simulations were performed using the Lamarckian-Genetic Algorithm (LGA) method with default parameters, generating 1000 conformations per compound (Abu Bakar *et al*., 2017). Post-analysis visualization of the molecular docking dataset was performed using BIOVIA Discovery Studio Visualizer.

RESULTS AND DISCUSSION

Synthesis and characterization of $[N^nBu_4]_2[Pd_2I_6]$

The synthesis of $[N^nBu_4]_2[Pd_2I_6]$ involved treating an acetone solution of $[N^nBu_4]I$ and I_2 with Pd metal powder at room temperature for 3 hr. The resulting black crystalline product (89% yield) was isolated by filtration, washed with diethyl ether (Et_2O), and air-dried. A second crop of the product was obtained by allowing Et_2O to diffuse into the acetone leachate over 3 days. An expedited crystallization method was employed to yield a product with reduced crystallinity while maintaining consistent analytical properties. This was achieved by adding ethanol and reducing the solvent volume until precipitation occurred.

The physical properties and analytical data of $[N^nBu_4]_2[Pd_2I_6]$ are summarized in Table 1. The elemental composition of the compound was determined using elemental analysis. The results indicated that the percentages of carbon (C), hydrogen (H), and nitrogen (N) in the compound closely matched the calculated values, demonstrating the accuracy and composition of $[N^nBu_4]_2[Pd_2I_6]$. The compound exhibits a melting point range of 198-231°C.

Table 1. Analytical and physical data of $[N^nBu_4]_2[Pd_2I_6]$

Complex	Exp.(calc)%			Color	Yield (%)	Melting point (°C)
	C	H	N			
$[N^nBu_4]_2[Pd_2I_6]$ $(C_{32}H_{72}I_6N_2Pd_2)$	26.8 (26.3)	5.1 (4.9)	2.0 (1.9)	Black	89 (130 mg)	198-213

The electronic spectra of $[N^nBu_4]_2[Pd_2I_6]$ were acquired in MeCN solution at ambient temperature across the wavelength range of 300-800 nm (Table 2). The compound exhibited three primary electronic excitation bands attributed to transitions from lower-lying 'd' orbitals to the empty $d_{x^2-y^2}$ orbital (Biyala *et al*., 2004). Pd(II) complexes with square planar configuration typically displayed three characteristic d-d transition bands in the ranges of 460–520 nm, 405–420 nm, and 320–380 nm corresponding to transitions from the ground state ($^1A_{1g}$) to the excited states $^1A_{2g}$, $^1B_{1g}$ and $^1E_{1g}$, respectively (Zianna *et al*., 2019). In the case of $[N^nBu_4]_2[Pd_2I_6]$, the observed bands are nearby or appear to overlap with previously reported spectral data (Tonde *et al*., 2005; Cuscusa *et al*., 2017; Jantan *et al*., 2024).

Table 2. The main absorbance bands nm (cm^{-1}) of $[N^nBu_4]_2[Pd_2I_6]$ and their assignment

Complex	ν (cm^{-1})	Λexp (nm)	ε, (dm^3moL^{-1} cm^{-1})	Electronic transition
$[N^nBu_4]_2[Pd_2I_6]$	29585	338	25347	$^1A_{1g}$ - $^1E_{1g}$
	22727	440	5553	$^1A_{1g}$ – $^1B_{1g}$
	19011	526	445	$^1A_{1g}$ – $^1A_{2g}$

The IR spectra (Figure 2) revealed two distinct bands in the range of 2956 cm^{-1} to 2867 cm^{-1} which were attributed to the asymmetric and symmetric sp^3 -CH_2 and -CH_3 stretching of aliphatic tetrabutylammonium moiety (Hashemian *et al*., 2013). The tetra-substituted carbon straight chain's prominent C-H bending vibrations were observed between 1456 cm^{-1} and 1377 cm^{-1} (Majid *et al*., 2019). The presence of C-N stretching features was confirmed by a weak band observed in the 1250 cm^{-1}-1020 cm^{-1} region. However, the stretching frequencies associated with Pd-I bonds were not detected, likely due to their absorption occurring at lower frequencies below 300 cm^{-1} (Rutherford *et al*.,1984).

The NMR spectrum (Figure 3) exhibits characteristic resonances corresponding to the $[N^nBu_4]^{2+}$ counter ion in acetone-d_6. A triplet resonance typical of a primary alkyl group was observed at 1.01 ppm, while signals attributable to secondary alkyl groups were detected at 1.52 ppm and 1.88 ppm in the ^1H NMR spectrum. The splitting pattern observed at 3.52 ppm in the spectra was assigned to the proton adjacent to the nitrogen group. Virtually unchanged carbon nuclei of $[N^nBu_4]^{2+}$ counterions compared to precursors were recorded in the ^{13}C NMR spectrum (Datta *et al*., 2017).

The thermogravimetric analysis (TGA) curve of $[N^nBu_4]_2[Pd_2I_6]$ displayed three distinct decomposition phases (Figure 4). Initially, a gradual decrease in mass was observed from 30°C to 220°C, which was attributed to the process of dehydration. This was followed by the first decomposition step occurring between 220°C and 315°C, resulting in a weight loss of 38% which was related to the decomposition of organic matter for $[N^nBu_4]^+$. The second decomposition step occurred in the temperature range of 315°C to 375°C, with a weight loss of 30% associated with the breakdown of the metal complex. Finally, the third decomposition step occurred between 375°C and 540°C, resulting in a weight loss of 29%. This loss has been attributed to the burning of decomposed material, which led to the formation of residue (Barbosa *et al*., 2017).

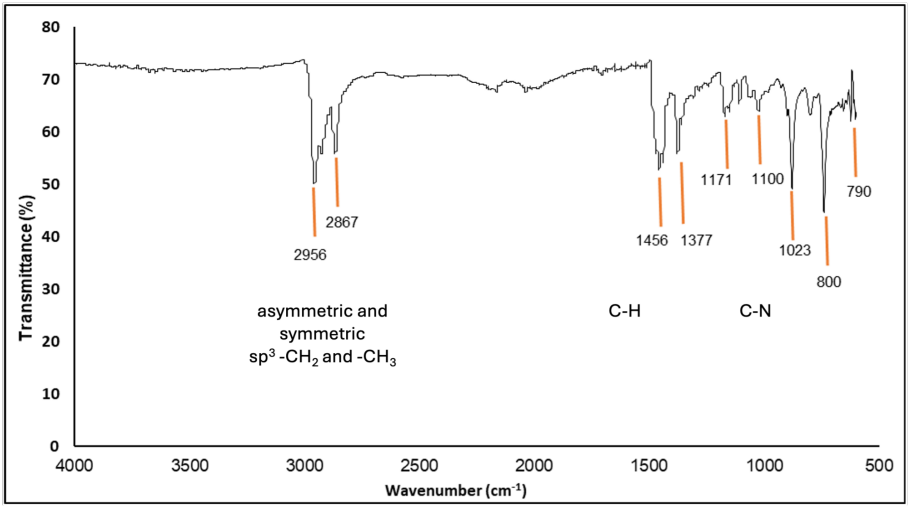

Fig. 2. FT-IR spectrum of $[N^nBu_4]_2[Pd_2I_6]$

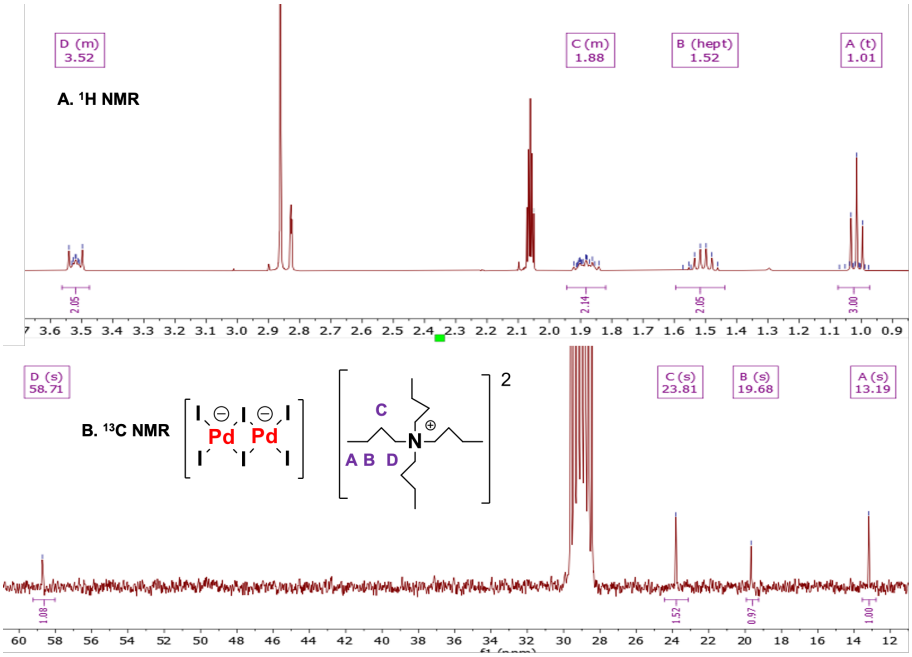

Fig. 3. (A) ^{1}H NMR, (B) ^{13}C NMR spectrum of $[N^nBu_4]_2[Pd_2I_6]$

Antimicrobial studies

Figure 5 depicts the iodide-bridged dimeric palladium complex's antimicrobial inhibition zones (in mm) against six bacterial strains at four distinct concentrations (1, 2, 3, 4 mg/mL). The measurements were conducted following overnight bacterial incubation at 37°C. The compound demonstrated adequate sensitivity against all tested bacterial species, exhibiting varying degrees of inhibitory activity ranging from 7.00 to 13.00 mm across all concentrations, with the optimum concentration of 3 mg/mL. The observed differences in inhibitory zones could be attributed to the fact that the tested Gram-positive and –negative bacterial cell walls interacted differently with $[N^nBu_4]_2[Pd_2I_6]$. Another possible explanation of our findings is that the complex may damage the bacterial cell membrane, leading to the leakage of intracellular contents and cell death. Previous studies have reported that palladium complexes can bind to proteins, resulting in DNA damage and subsequent cell death (Lacerda *et al*., 2022). *B. subtilis* has shown significant increases in a concentration-dependent manner compared to *S. typhimurium.* The positive control Gentamicin (10 µg) employed in this study showed an inhibition range of 22.0 to 25.0 mm.

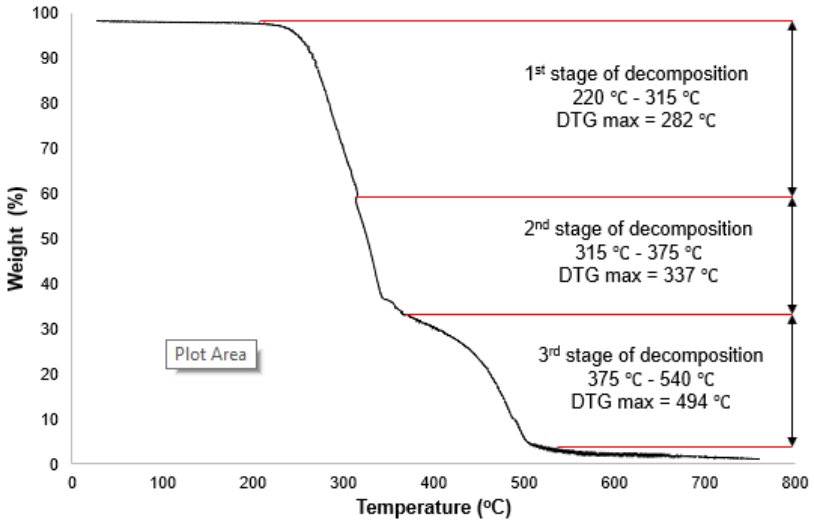

Fig. 4. TGA Plot Area of $[N^nBu_4]_2[Pd_2I_6]$

This study highlights a potential correlation between the structure of metal complexes and their chelation behavior, facilitating their efficacy as potent antibacterial agents through bacterial growth suppression. Palladium nanoparticles have been documented to show more significant growth inhibition against *S. aureus*, compared to *E. coli* (Adams *et al*., 2014). These results align with our findings, highlighting the complex as a useful antimicrobial agent, especially for Gram-positive bacteria, *B. subtilis*. Nevertheless, possible toxicity is a challenge to safety. Thus, as a result of this part of the investigation, further work, such as cytotoxicity against mammalian cell lines, could be needed to clarify the applicability of $[N^nBu_4]_2[Pd_2I_6]$ therapy in clinical practice.

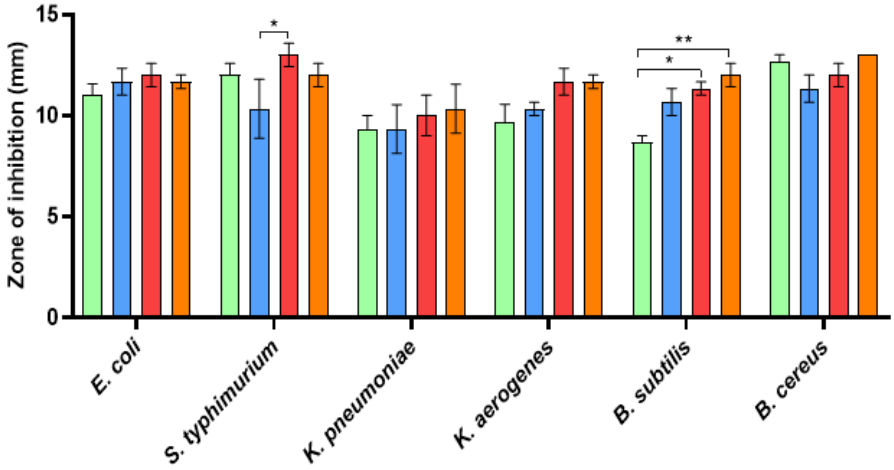

Fig. 5. Disk diffusion susceptibility assay of six tested bacteria to $(N^nBu_4)_2[Pd_2I_6]$ at 1mg/mL, 2mg/mL, 3mg/mL, and 4mg/mL. The levels displayed are the mean of three tested cultures ± SEM. The asterisks indicate statistically significant differences analyzed with two-way ANOVA followed by Tukey's multiple comparison post-test

Table 3 represents the MIC and MBC results of $[N^nBu_4]_2[Pd_2I_6]$ against *E. coli*, *S. typhimurium*, *K. pneumoniae*, *K. aerogenes*, *B. subtilis* and *B. cereus* bacterial strains using the broth dilution method. MIC values reflect the lowest concentration of the compound that prevents microbial growth, indicated by the absence of turbidity after 24 hr of incubation. The compound demonstrated the highest susceptibility against both *Klebsiella* species, with the lowest MIC recorded at 0.625 mg/mL. Both Gram-positive *Bacillus* species and Gram-negative *S. typhimurium* displayed MIC values of 1.25 mg/mL. In contrast, the compound exhibited lower antibacterial activity against *E. coli*, with a MIC of 2.5 mg/mL.

Table 3. MIC and MBC of $(N^nBu_4)_2[Pd_2I_6]$ against selected bacterial strains

Bacterial Strains	MIC (mg/mL)	MBC(mg/mL)
E. coli	2.5	+
S. typhimurium	1.25	+
K. pneumoniae	0.625	+
K. aerogenes	0.625	1.25
B. subtilis	1.25	+
B. cereus	1.25	+

(+) = evidence of bacterial growth

Additionally, MBC values were determined to establish the minimum concentration required for bacterial eradication. Following the MIC analysis, the samples were streaked onto MHA plates. Experimental findings revealed that only *K. aerogenes* exhibited the highest sensitivity to the compound, demonstrating effective bactericidal activity at an MBC of 1.25 mg/mL. Other studied bacterial species exhibited growth, indicating no bactericidal activity when exposed to the complex.

ADMET profiles, drug-likeness, and Protox-III analysis

Selecting a metal-based complex for synthesis, characterization, testing, and development as a therapeutic candidate involves evaluating crucial physicochemical properties, lipophilicity, water solubility, pharmacokinetics, drug-likeness, medicinal chemistry, and toxicity. In this study, $[N^nBu_4]_2[Pd_2I_6]$ underwent comprehensive analysis using SwissADME and ProTox-3.0 online servers, with key parameters summarized in Table 4.

The compound features 24 rotatable bonds based on its physicochemical characteristics. Notably, lipophilicity values indicate zero for $LogP_{o/w}$ (iLOGP) and 15.73 for $LogP_{o/w}$ (XLOGP3). Predictions suggest limited permeability across the blood-brain barrier and minimal absorption in the gastrointestinal tract. The compound exhibits non-compliance with Lipinski's rule of 5 (molecular weight ≤ 500, octanol-water partition coefficient logP ≤ 5, hydrogen bond donors ≤ 5, and hydrogen bond acceptors ≤ 10), potentially explaining its low permeability and absorption. Moreover, predictive models developed by Ghose, Veber, and Muegge suggest that the compound lacks drug-like properties due to rule violations. The $[N^nBu_4]_2[Pd_2I_6]$ complex demonstrates favorable drug-like properties as indicated by models proposed by Lipinski and Egan. These properties, including molecular stability and specific pharmacophoric characteristics, suggest its potential drug-likeness. Although the complex does not strictly conform to all aspects of Lipinski's rule of five, it aligns with key principles that support its viability as a drug candidate (Benet *et al*. 2016). These characteristics highlight the $[N^nBu_4]_2[Pd_2I_6]$ complex's promise for further development in drug discovery.

The medicinal parameters analysis revealed no alerts by PAINS (Pan Assay Interference compounds) and two alerts by Brenk, likely attributed to the presence of iodine and quaternary nitrogen molecules in the compound. The predicted lethal dose value (LD_{50}) for $[N^nBu_4]_2[Pd_2I_6]$ was determined to be 189 mg/kg body weight, corresponding to a predicted toxicity class of 3. This classification indicates that the compound could be toxic if ingested (50 mg/kg < LD_{50} < 300 mg/kg).

Molecular docking

Staphylococcus aureus has been well-established as a primary bacterial pathogen responsible for significant human diseases. In this essay, visualization of the docked confirmation of $[N^nBu_4]_2[Pd_2I_6]$ interaction with the TMK protein active binding site of *S. aureus* was shown in Figure 6. Lower binding energies indicate the stronger binding affinity of the compound with the target protein (Khan *et al*., 2023). $[N^nBu_4]_2[Pd_2I_6]$ preferable ligand-protein interaction was shown to be buried deep inside the pocket region of TMK, resulting in free binding energy of -9.90 kcaL/moL with an inhibition constant (Ki) of 54.96 nM against 4GFD protein. The docking results demonstrate a high binding affinity between the $[N^nBu_4]_2[Pd_2I_6]$ complex and TMK, indicating strong interactions likely to inhibit the enzyme's activity effectively. The analysis highlights specific interactions between the $[N^nBu_4]_2[Pd_2I_6]$ complex and key active site residues of TMK, including hydrogen bonds, hydrophobic contacts, and van der Waals interactions, stabilizing the inhibitor within the active site. The binding of the $[N^nBu_4]_2[Pd_2I_6]$ complex to TMK's active site can lead to either competitive inhibition, where it competes with dTMP for binding, or allosteric inhibition, where it induces conformational changes that reduce enzyme activity. This disruption may trigger a cascade of cellular events, including replication stress and activation of DNA damage response pathways, ultimately leading to bacterial cell death (Gonzalez-Prada *et al*. 2024). Overall, the values obtained from this analysis indicated that the binding process is spontaneous and

that the compound can be accepted as an active pharmaceutical ingredient drug (Hadhoum *et al*., 2021).

Table 4. ADMET and drug-likeness parameters predicted by SwissADME and ProTox-3.0

ADME data	
Physicochemical	
Formula	$C_{32}H_{72}I_6N_2Pd_2$
Molecular weight	1459.19 g/moL
Number of rotatable bonds	24
Lipophilicity	
Log $P_{o/w}$ (iLOGP)	0.00
Log $P_{o/w}$ (XLOGP3)	15.73
Water Solubility	
Solubility	8.94 x 10^{-15} mg/mL
Class	Insoluble
Pharmacokinetics	
Blood-brain barrier permeant (BBB P)	Low
Gastrointestinal absorption (GI A)	No
Drug Likeness	
Lipinski	Yes; 1 violation: MW>500
Ghose	No; 4 violations: MW>480, WLOGP<-0.4, MR>130, #atoms>70
Veber	No; 1 violation: Rotors>10
Egan	Yes
Muegge	No; 3 violations: MW>600, XLOGP3>5, Rotors>15
Medicinal Chemistry	
PAINS	0 alert
Brenk	2 alert: iodine, quaternary nitrogen
ProTox-3.0	
Toxicity of chemicals	
Predicted LD50	189 mg/kg
Predicted Toxicity	Class 3
Number of hydrogen bond acceptors	0
Number of hydrogen bond donors	0
Octanol/water partition coefficient (logP)	-7.97

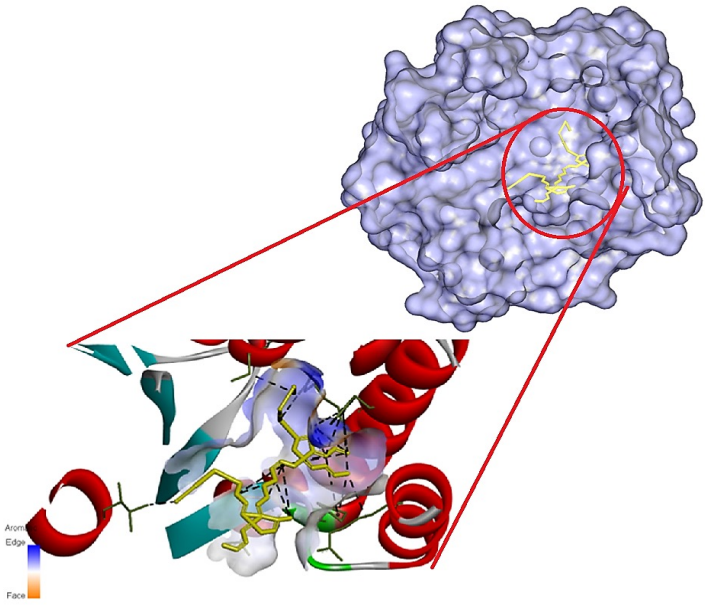

Fig. 6. View of docked conformation of $[N^nBu_4]_2[Pd_2I_6]$ with TMK from *S. aureus* protein

The detailed compound-binding site interaction in 2D structural views is shown in Figure 7. Iodine atoms of $[N^nBu_4]_2[Pd_2I_6]$ interact with *Ser A96* (4.15 Å) and *Arg A70* (5.96 Å) through carbon-hydrogen

and conventional hydrogen bonds, respectively. Interestingly, Pd atoms were involved in metal-acceptor interactions with Thr A16 (4.10 Å). The tetrabutylammonium moiety made attractive alkyl and π -alkyl interaction with *Phe A66*, *Pro A38,* and *Arg A48*. Furthermore, the compound is surrounded by residue *Gln A101*, *Tyr A100*, *Ser A97*, *Ser A69*, *ASP A91*, *ARG A36,* and *LYS A15*, leading to favorable Van Der Waals interactions, thus increasing its affinity for TMK protein.

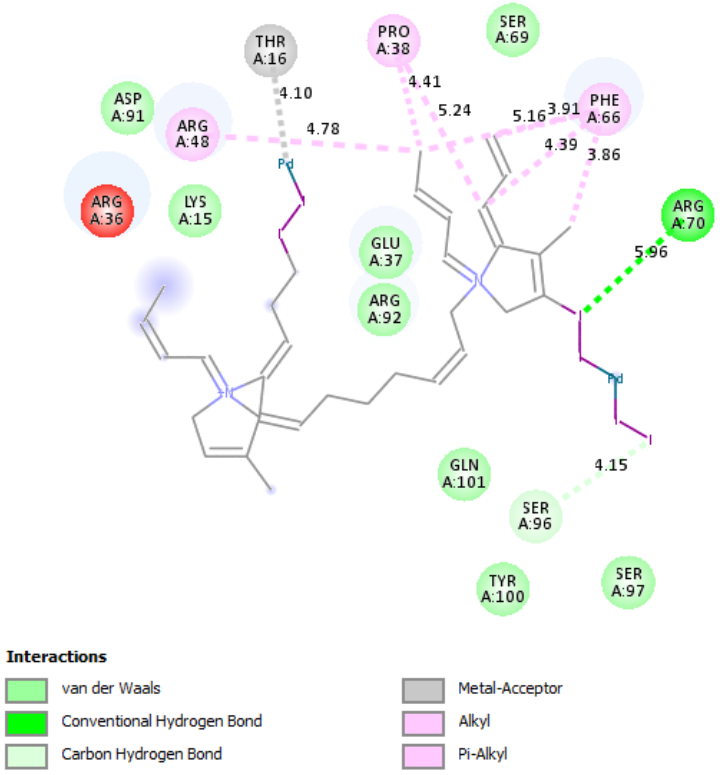

Fig. 7. 2-dimensional visual interactions between $[N^nBu_4]_2[Pd_2I_6]$ and TMK protein residues from *S. aureus*

CONCLUSION

This research explores the direct application of an iodide-bridged dimeric palladium complex as a potential antibacterial agent. Various spectroscopic techniques were utilized to confirm the complex's formulation. The $[N^nBu_4]_2[Pd_2I_6]$ were screened for their antibacterial efficacy under laboratory conditions against *Bacillus cereus*, *Bacillus subtilis*, *Salmonella typhimurium*, *Escherichia coli*, *Klebsiella aerogenes*, and *Klebsiella pneumoniae*. The antibacterial activity analysis indicated that the complex exhibits effective antimicrobial activity, with varying sensitivity levels among different tested microbial species with prominent inhibition rather than killing effect. The simulated computational toxicity analysis provides insights into the pharmacokinetics and toxicity of the compounds. Overall, $[N^nBu_4]_2[Pd_2I_6]$ exhibits limited absorption and permeability but possesses favorable drug-like properties according to Lipinski's and Egan's criteria. Despite two Brenk alerts, there is no PAINS interference. The molecular docking analysis also elucidates the compound's mechanistic interaction with TMK, identifying the protein's favorable binding region and the involved amino acid residues. This strong interaction between the compound and TMK suggests the formation of a stable and rational interaction complex.

ACKNOWLEDGEMENTS

The author acknowledges the support and funding provided by the Ministry of Higher Education, Malaysia, and Universiti Teknologi MARA through a scholarship under the Post-Doctoral Training Scheme (grant code: KPT(BS)820710105709) and financial assistance via the Fundamental Research Grant Scheme (FRGS)-RACER (grant code: RACER/1/2019/STG07/UITM//6). The authors express gratitude to the Faculty of Applied Sciences at UiTM and the Department of Chemistry at Imperial College London for their generous support and provision of research facilities.

CONFLICT OF INTEREST

The authors declare no conflict of interest.

ETHICAL STATEMENT

Not applicable

REFERENCES

Abu Bakar, A. R., Manaharan, T., Merican, A.F. & Mohamad, S.B. 2017. Experimental and computational approaches to reveal the potential of *Ficus deltoidea* leaves extract as α-amylase inhibitor. Natural Product Research, 32(4): 473–476. https://doi.org/10.1080/14786419.2017.1312393

Adams, C.P., Walker, K.A., Obare, S.O. & Docherty, K.M. 2014. Size-dependent antimicrobial effects of novel palladium nanoparticles. PLoS ONE, 9(1): e85981. https://doi.org/10.1371/journal.pone.0085981

Agu, P.C., Afiukwa, C.A., Orji, O.U., Ezeh, E.M., Ofoke, I.H., Ogbu, C.O., Ugwuja, E.I. & Aja, P.M. 2023. Molecular docking as a tool for the discovery of molecular targets of nutraceuticals in diseases management. Scientific Reports, 13(1): 13398. https://doi.org/10.1038/s41598-023-40160-2

Aljohani, F.S., Abu-Dief, A.M., El-Khatib, R.M., Al-Abdulkarim, H.A., Alharbi, A., Mahran, A. & El-Metwaly, N.M. 2021. Structural inspection for novel Pd (II), VO (II), Zn (II) and Cr (III)-azomethine metal chelates: DNA interaction, biological screening and theoretical treatments. Journal of Molecular Structure, 1246: 131139. https://doi.org/10.1016/j.molstruc.2021.131139

Balaram, V. 2019. A review of applications, occurrence, exploration, analysis, recycling, and environmental impact. Geoscience Frontiers, 10(4): 1285-1303. https://doi.org/10.1016/j.gsf.2018.12.005

Barbosa, H.F.G., Attjioui, M., Ferreira, A.P.G., Dockal, E.R., El Gueddari, N.E., Moerschbacher, B.M., & Cavalheiro, É.T.G. 2017. Synthesis, characterization and biological activities of biopolymeric schiff bases prepared with chitosan and salicylaldehydes and their Pd (II) and Pt (II) complexes. Molecules, 22(11): 1987. https://doi.org/10.3390/molecules22111987

Biyala, M.K., Fahmi, N. & Singh, R.V. 2004. Preparation, characterization and antimicrobial properties of some palladium and platinum complexes with active Schiff base ligands. Indian Journal of Chemistry, 43(12): 2536-2541.

Benet, L.Z., Hosey, C.M., Ursu, O. & Oprea, T.I. 2016. BDDCS, the Rule of 5 and drugability. Advanced Drug Delivery Reviews, 101: 89–98. https://doi.org/10.1016/j.addr.2016.05.007

Cowley, A., Jiang, J., Tang, B. & Wang, A. 2022. PGM Market Report. Jonhson Matthey.

Cuscusa, M., Rigoldi, A., Artizzu, F., Cammi, R., Fornasiero, P., Deplano, P. & Serpe, A. 2017. Ionic couple-driven palladium leaching by organic triiodide solutions. ACS Sustainable Chemistry & Engineering, 5(5): 4359-4370. https://doi.org/10.1021/acssuschemeng.7b00410

Daina, A., Michielin, O. & Zoete, V. 2017. SwissADME: a free web tool to evaluate pharmacokinetics, drug-likeness and medicinal chemistry friendliness of small molecules. Scientific Reports, 7(1): 42717. https://doi.org/10.1038/srep42717

Datta, B., Roy, A. & Roy, M. N. 2017. Inclusion complexation of tetrabutylammonium iodide by cyclodextrins. Journal of Chemical Sciences, 129(5): 579-587. https://doi.org/10.1007/s12039 -017-1267-5

Dechouk, L.F., Bouchoucha, A., Abdi, Y., Larbi, K.S., Bouzaheur, A. &Terrachet-Bouaziz, S. 2022. Coordination of new palladium (II) complexes with derived furopyran-3, 4-dione ligands: Synthesis, characterization, redox behaviour, DFT, antimicrobial activity, molecular docking and ADMET studies. Journal of Molecular Structure, 1257: 132611. https://doi.org/10.1016/j.molstruc.2022.132611

Dhingra, S., Rahman, N.A.A., Peile, E., Rahman, M., Sartelli, M., Hassali, M.A., Islam, T., Islam, S. & Haque, M. 2020. Microbial resistance movements: an overview of global public health threats posed by antimicrobial resistance, and how best to counter. Frontiers in Public Health, 8: 535668. https://doi.org/10.3389/fpubh.2020.535668

Drwal, M.N., Banerjee, P., Dunkel, M., Wettig, M.R. & Preissner, R. 2014. ProTox: a web server for the *in silico* prediction of rodent oral toxicity. Nucleic Acids Research, 42(W1): W53-W58. https://doi.org/10.1093/nar/gku401

Egan, W. J., Merz, K. M. & Baldwin, J.J. 2000. Prediction of drug absorption using multivariate statistics. Journal of Medicinal Chemistry, 43(21): 3867-3877. https://doi.org/10.1021/jm000292e

Frei, A., Zuegg, J., Elliott, A.G., Baker, M., Braese, S., Brown, C., Chen, F., Dowson, C.G., Dujardin, G., Jung, N. & King, A.P. 2020. Metal complexes as a promising source for new antibiotics. Chemical Science, 11(10): 2627-2639. https://doi.org/10.1039/C9SC06460E

Frei, A., Verderosa, A.D., Elliott, A.G., Zuegg, J. & Blaskovich, M.A. 2023. Metals to combat antimicrobial

resistance. Nature Reviews Chemistry, 7(3): 202-224. https://doi.org/10.1038/s41570-023-00463-4

Fuzi, N.A.N.M., Rahmat, S.K., Aziz, M.H.A., Jalil, M.N., Ali, S.B.G. & Jantan, K.A. 2023. Recovered palladium complexes as a potential homogeneous catalyst for CH functionalization and antibacterial agent. Malaysian Journal of Analytical Sciences, 27(2): 407-421.

Ghose, A.K., Viswanadhan, V.N. & Wendoloski, J.J. 1999. A knowledge-based approach in designing combinatorial or medicinal chemistry libraries for drug discovery. 1. A qualitative and quantitative characterization of known drug databases. Journal of Combinatorial Chemistry, 1(1): 55-68. https://doi.org/10.1021/cc9800071

Gombac, V., Montini, T., Falqui, A., Loche, D., Prato, M., Genovese, A., Mercuri, M.L., Serpe, A., Fornasiero, P. & Deplano, P. 2016. From: Trash to resource: Recovered-Pd from spent three-way catalysts as a precursor of an effective photo-catalyst for H_2 production. Green Chemistry, 18(9): 2745–2752. https://doi.org/10.1039/c5gc02908b

Gonzalez-Prada, I., Borges, A., Santos-Torres, B., Magariños, B., Simões, M., Concheiro, A. & Alvarez-Lorenzo, C. 2024. Antimicrobial cyclodextrin-assisted electrospun fibers loaded with carvacrol, citronellol and cinnamic acid for wound healing. International Journal of Biological Macromolecules, 277: 134154. https://doi.org/10.1016/j.ijbiomac.2024.134154

Hadhoum, N., Hadjadj-Aoul, F. Z., Hocine, S., Bouaziz-Terrachet, S., Abdoun, A., Seklaoui, N., Boubrit, F., Abderrahim, W. & Mekacher, L.R. 2021. Design and one-pot synthesis of some new [3, 5-di (4', 5'-diphenyl-2'-substituted)-1h-imidazol-1-yl)]-1h-1, 2, 4-triazole derivatives: *In silico* admet and docking study, antibacterial and antifungal activities evaluation. Heterocycles, 102(10): 1949-1968. https://doi.org/10.3987/COM-21-14503

Hashemian, S., Sadeghi, B., Mozafari, F., Salehifar, H. & Salari, K. 2013. Adsorption of disperse of yellow 42 onto bentonite and organo-modified bentonite by tetra butyl ammonium iodide (B-TBAI). Polish Journal of Environmental Studies, 22(5): 1363-1370.

Jantan, K.A., Kwok, C.Y., Chan, K.W., Marchiò, L., White, A.J.P., Deplano, P., Serpe, A. & Wilton-Ely, J.D.E.T. 2017. From recovered metal waste to high-performance palladium catalysts. Green Chemistry, 19(24): 5846-5853. https://doi.org/10.1039/C7GC02678A

Jantan, K.A., Ekart, G., McCarthy, S., White, A.J.P., Braddock, D.C., Serpe, A. & Wilton-Ely, J.D.E.T. 2024. Palladium complexes derived from waste as catalysts for C-H functionalisation and C-N bond formation. Catalysts, 14(5): 295. https://doi.org/10.3390/catal14050295

Jayanthi, K. & Azam, M.A. 2023. Thymidylate kinase inhibitors as antibacterial agents: A review. Applied Biochemistry and Microbiology, 593: 250-266. https://doi.org/10.1134/S0003683823030092

Kawatkar, S.P., Keating, T.A., Olivier, N.B., Breen, J.N., Green, O.M., Guler, S.Y., Hentemann, M.F., Loch, J.T., McKenzie, A.R., Newman, J.V. & Otterson, L.G. 2014. Antibacterial inhibitors of gram-positive thymidylate kinase: Structure–activity relationships and chiral preference of a new hydrophobic binding region. Journal of Medicinal Chemistry, 57(11): 4584-4597. https://doi.org/10.1021/jm500463c

Khan, H., Sirajuddin, M., Badshah, A., Ahmad, S., Bilal, M., Salman, S. M., Butler, I.S., Wani, T.A. & Zargar, S. 2023. Synthesis, physicochemical characterization, biological evaluation, *in silico* and molecular docking studies of Pd (II) complexes with P, S-donor ligands. Pharmaceuticals, 16(6): 806. https://doi.org/10.3390/ph16060806

Lacerda, M.L.D., Rossi, D.A., Lourenzatto, E.C.A., Takeuchi, M.G., Souza, W.A., Silva, R.T.C., Julio, L.G., Guerra, W., & Melo, R.T.D. 2022. Antimicrobial resistance challenged with Platinum (II) and Palladium (II) complexes containing 1, 10-phenanthroline and 5-Amino-1, 3, 4-Thiadiazole-2 (3H)-Thione in *Campylobacter jejuni*. Antibiotics, 11(11): 1645. https://doi.org/10.3390/antibiotics11111645

Lipinski, C.A., Lombardo, F., Dominy, B.W. & Feeney, P.J. 1997. Experimental and computational approaches to estimate solubility and permeability in drug discovery and development settings. Advanced Drug Delivery Reviews, 23(1-3): 3-25. https://doi.org/10.1016/j.addr.2012.09.019

Majid, M.F., Zaid, H.F.M., Kait, C.F., Abd Ghani, N. & Jumbri, K. 2019. Mixtures of tetrabutylammonium chloride salt with different glycol structures: Thermal stability and functional groups characterizations. Journal of Molecular Liquids, 294: 111588. https://doi.org/10.1016/j.molliq.2019.111588

Moulijn, J.A., Van Diepen, A.E. & Kapteijn, F. 2001. Catalyst deactivation: Is it predictable?: What to do?. Applied Catalysis A: General, 212(1-2): 3-16. https://doi.org/10.1016/S0926-860X(00)00842-5

Morris, G.M., Huey, R., Lindstrom, W., Sanner, M.F., Belew, R.K., Goodsell, D.S. & Olson, A.J. 2009. AutoDock4 and AutoDockTools4: Automated docking with selective receptor flexibility. Journal of Computational Chemistry, 30(16): 2785–2791. https://doi.org/10.1002/jcc.21256

Muegge, I. 2002. Pharmacophore features of potential drugs. Chemistry–A European Journal, 8(9):

1976-1981. https://doi.org/10.1002/1521-3765(20020503)8:9<1976::AID-CHEM1976>3.0.CO;2-K

Oliveira, W.X., da Costa, M.M., Fontes, A.P., Pinheiro, C.B., de Paula, F.C., Jaimes, E.H., Pedroso, E.F., de Souza, P.P., Pereira-Maia, E.C. & Pereira, C.L. 2014. Palladium (II) and platinum (II) oxamate complexes as potential anticancer agents: Structural characterization and cytotoxic activity. Polyhedron, 76: 16-21. https://doi.org/10.1016/j.poly.2014.03.049

Rutherford, N.M., Olmstead, M.M. & Balch, A.L. 1984. Bridged or nonbridged structures for dinuclear metal complexes. The case of tetrakis (methyl isocyanide) dipalladium (I) iodide: An unbridged compound. Inorganic Chemistry, 23: 2833-2837. https://doi.org/10.1021/ic00186a024

Robinson, B.H. 2009. E-waste: An assessment of global production and environmental impacts. Science of The Total Environment, 408(2): 183-191. https://doi.org/10.1016/j.scitotenv.2009.09.044

Serpe, A., Bigoli, F., Cabras, M.C., Fornasiero, P., Graziani, M., Mercuri, M.L., Montini, T., Pilia, L., Trogua E.F. & Deplano, P. 2005. Pd-Dissolution through a mild and effective one-step reaction and its application for Pd-recovery from spent catalytic converters. Chemical Communication, 8:1040-1042. https://doi.org/10.1039/B415799K

Soldevila-Barreda, J.J. & Metzler-Nolte, N. 2019. Intracellular catalysis with selected metal complexes and metallic nanoparticles: advances toward the development of catalytic metallodrugs. Chemical Reviews, 119(2): 829-869. https://doi.org/10.1021/acs.chemrev.8b00493

Tonde, S.S., Kelkar, A.A., Bhadbhade, M.M. & Chaudhari, R.V. 2005. Isolation and characterization of an iodide bridged dimeric palladium complex in carbonylation of methanol. Journal of Organometallic Chemistry, 690: 1677-1681.

Veber, D.F., Johnson, S.R., Cheng, H.Y., Smith, B.R., Ward, K.W. & Kopple, K.D. 2002. Molecular properties that influence the oral bioavailability of drug candidates. Journal of Medicinal Chemistry, 45(12): 2615-2623. https://doi.org/10.1021/jm020017n

Yang, H., Lou, C., Sun, L., Li, J., Cai, Y., Wang, Z., Li, W., Liu, G. & Tang, Y. 2019. admetSAR 2.0: Web-service for prediction and optimization of chemical ADMET properties. Bioinformatics, 35(6): 1067-1069. https://doi.org/10.1093/bioinformatics/bty707

Zalevskaya, O., Gur'eva, Y., Kutchin, A. & Hansford, K.A. 2020. Antimicrobial and antifungal activities of terpene-derived palladium complexes. Antibiotics, 9(5): 277. https://doi.org/10.3390/antibiotics9050277

Zianna, A., Geromichalos, G.D., Pekou, A., Hatzidimitriou, A.G., Coutouli-Argyropoulou, E., Lalia-Kantouri, M., Pantazaki, A.A. & Psomas, G. 2019. A palladium (II) complex with the Schiff base 4-chloro-2-(N-ethyliminomethyl)-phenol: Synthesis, structural characterization, and in vitro and in silico biological activity studies. Journal of Inorganic Biochemistry, 199: 110792. https://doi.org/10.1016/j.jinorgbio.2019.110792